UC Davis

UC Davis Previously Published Works

Title

Using computer-extracted image phenotypes from tumors on breast magnetic resonance imaging to predict breast cancer pathologic stage.

Permalink

https://escholarship.org/uc/item/3m269456

Journal

Cancer, 122(5)

Authors

Burnside, Elizabeth
Drukker, Karen
Li, Hui
et al.

Publication Date

2016-03-01

DOI

10.1002/cncr.29791

Peer reviewed

eScholarship.org Powered by the California Digital Library
University of California

Author Manuscript

Author Manuscript

Author Manuscript

Author Manuscript

HHS Public Access

Author manuscript

Cancer. Author manuscript; available in PMC 2017 March 01.

Published in final edited form as:

Cancer. 2016 March 1; 122(5): 748–757. doi:10.1002/cncr.29791.

Using Computer-extracted Image Phenotypes from Tumors on Breast MRI to Predict Breast Cancer Pathologic Stage

Elizabeth S. Burnside, MD, MPH, MS[*,1], **Karen Drukker, PhD, MBA**[*,2], **Hui Li, PhD**[2], **Ermelinda Bonaccio, M.D.**[3], **Margarita Zuley, M.D.**[4], **Marie Ganott, M.D.**[4], **Jose M. Net, M.D.**[5], **Elizabeth Sutton, M.D.**[6], **Kathleen R. Brandt, M.D.**[7], **Gary Whitman, M.D.**[8], **Suzanne Conzen, M.D.**[2], **Li Lan, MS**[2], **Yuan Ji, PhD**[9,10], **Yitan Zhu, PhD**[10], **Carl Jaffe, MD**[11], **Erich Huang, Ph.D.**[11], **John Freymann**[11], **Justin Kirby**[11], **Elizabeth Morris, MD**[‡,6], and **Maryellen Giger, PhD**[‡,2]

[1]Department of Radiology, University of Wisconsin School of Medicine and Public Health Wisconsin, US

[2]Department of Radiology, University of Chicago, Chicago, IL

[3]Department of Radiology, Roswell Park Cancer Institute, Buffalo, NY

[4]Department of Radiology, University of Pittsburgh, Pittsburgh, PA

[5]University of Miami, Miller School of Medicine, Miami, FL

[6]Memorial Sloan Kettering Cancer Center, New York, NY

[7]Mayo Clinic, Rochester, MN

[8]MD Anderson Cancer Center, Houston, TX

[9]Department of Health Studies, University of Chicago, Chicago, IL

[10]Program of Computational Genomics & Medicine, NorthShore University HealthSystem, Evanston, IL

[11]National Cancer Institute, National Institutes of Health, Rockville, MD

Abstract

Background—To demonstrate that computer-extracted image phenotypes (CEIPs) of biopsy-proven breast cancer on MRI can accurately predict pathologic stage.

Methods—We used a dataset of de-identified breast MRIs organized by the National Cancer Institute in The Cancer Imaging Archive. We analyzed 91 biopsy-proven breast cancer cases with pathologic stage (stage I = 22; stage II = 58; stage III = 11) and surgically proven nodal status

Corresponding Author contact information: Maryellen L. Giger, Ph.D., University of Chicago, Radiology MC 2026, 5841 S. Maryland Avenue, Chicago, IL 60637, Phone: 773-702-6778, m-giger@uchicago.edu.

*Drs. Burnside and Drukker are both first authors

‡Drs. Giger and Morris are both senior corresponding authors

Disclosures: Maryellen L.Giger is a stockholder in R2 technology/Hologic and receives royalties from Hologic, GE Medical Systems, MEDIAN Technologies, Riverain Medical, Mitsubishi and Toshiba. She is a cofounder of and stockholder in Quantitative Insights. Karen Drukker received royalties from Hologic.

The authors not mentioned with specific disclosures above declare no relationships with any companies, whose products or services may be related to the subject matter of the article.

Author Manuscript Author Manuscript Author Manuscript Author Manuscript

(negative nodes = 46, ≥ 1 positive node = 44, no nodes examined = 1). We characterized tumors by (a) radiologist measured size, and (b) CEIP. We built models combining two CEIPs to predict tumor pathologic stage and lymph node involvement, evaluated them in leave-one-out cross-validation with area under the ROC curve (AUC) as figure of merit.

Results—Tumor size was the most powerful predictor of pathologic stage but CEIPs capturing biologic behavior also emerged as predictive (e.g. stage I+II vs. III demonstrated AUC = 0.83). No size measure was successful in the prediction of positive lymph nodes but adding a CEIP describing tumor "homogeneity," significantly improved this discrimination (AUC = 0.62, p=.003) over chance.

Conclusions—Our results indicate that MRI phenotypes show promise for predicting breast cancer pathologic stage and lymph node status.

Keywords

breast cancer stage; prognosis; quantitative image analysis; MRI

Introduction[1]

Historically, one of the most important roles of imaging in women with breast cancer was to accurately predict stage in order to direct patients to appropriate treatment and provide accurate prognosis. At the time of diagnosis, imaging is primarily used to establish "clinical" stage (as defined by the American Joint Committee on Cancer 7th edition —AJCC 7) prior to surgical intervention, after which time "pathologic" stage drives further decision-making [1]. However, the TNM staging system in the era of biomarkers, genomic analysis, and personalized medicine is increasingly viewed as limited [2,3]. The emergence of tumor biology [4] as perhaps the most powerful factor driving prognosis has engendered substantial interest in understanding how biomarkers like those seen on breast MRI may help predict pathologic stage and thus inform optimal therapy.

Management decisions are driven by clinical stage including the use of whole-body imaging to evaluate for metastatic disease, election to undergo neoadjuvant chemotherapy, appropriate surgical management and radiation therapy planning [1]. In general, women with clinical stage III disease, in contrast to women with clinical stage I or II disease, have a higher risk for metastatic disease and thus routinely undergo systemic imaging; are candidates for neoadjuvant chemotherapy; and are less likely to be candidates for breast conservation therapy and sentinel node procedures [5]. As an example, the decision to proceed with neoadjuvant chemotherapy is necessarily a judgment based on clinical stage without knowledge of pathologic stage, thus is based primarily on imaging; with MRI often playing a key role. Breast MRI has been shown to be an accurate method for predicting extent of breast cancer [6] as well as demonstrating axillary lymph node involvement through direct evaluation of the axilla [7-10]. However, MRI may overestimate tumor size [11] and underestimate axillary lymph node involvement, therefore, imaging has not yet obviated the need for surgical staging including sentinel biopsy or axillary lymph node dissection [8].

[1]Abbreviations: CEIP: computer-extracted image phenotype, TCGA: The Cancer Genome Atlas, TCIA: The Cancer Imaging Archive

Author Manuscript Author Manuscript Author Manuscript Author Manuscript

Current research indicates that quantitative MRI tumor biomarkers, i.e., phenotypes, rather than anatomic evaluation, may hold promise in predicting malignancy [12-15], breast cancer subtypes [16-21] molecular pathways [22], gene expression[23,24] and lymph node status [10,25,26]. However, little literature is available to demonstrate whether computer-extracted MRI phenotypes, can augment prediction of pathologic stage. Our goal in this study was to determine whether computer extracted phenotypes of biopsy-proven breast cancer on MRI can predict breast cancer pathologic stage and which phenotypes are most important.

Material and Methods

Study population

All patient data used in this study were obtained under IRB-approved HIPAA compliant protocols. The current study had access to de-identified data only and the project derived cases from the cohort collected via The Cancer Genome Atlas—TCGA (https://tcga-data.nci.nih.gov) Breast Cancer (BRCA) initiative for which cases were solicited from five comprehensive cancer centers across the US. The TCGA was established to create a repository of tissue samples sufficient for deep genomic and proteomic analysis. Each tissue sample was required to contain 200-300 mg of tissue. Thus, for breast a surgical excision was necessary to obtain this amount of tissue. Each tissue sample was also required to be "treatment-naïve," therefore, each patient eligible for inclusion in the TCGA database could not have had preoperative treatment of any kind. Collection of MRI images followed, as a secondary initiative, after the tissue samples met the criteria for inclusion in the TCGA. At the time of our study, 1,078 breast cancer cases had been collected under the auspices of the ongoing TCGA initiative. Active collection of breast MRI data for a subset of these individuals had established an MRI dataset of 108 examinations made available in The Cancer Imaging Archive—TCIA (http://http://www.cancerimagingarchive.net). The majority of these breast MRI studies were performed following a breast cancer diagnosis established by image-guided core needle biopsy and all of the MRI examinations included in this study were performed prior to any treatment. Of these cases, 48 MRI cases had been previously analyzed by Mazurowski et al., who related MRI enhancement dynamics to the luminal B subtype, however the analysis was not conducted as part of the TCIA Breast Cancer group [22].

For our study, all breast MRI data were downloaded from the TCIA and clinical, pathological, and genetic information was compiled using TCGA assembler, a free open-source publicly available tool [27]. In order to impose imaging uniformity, we included the majority of breast MRI studies similar in acquisition and technique (1.5 Tesla magnet strength using GE Medical Systems, Milwaukee, Wisconsin, USA); a total of 93 cases. We excluded cases that had missing images (1 patient) or missing genetic data (1 patient). Hence, we included a data set of 91 breast MRI cases.

Image data

Breast MRIs analyzed in this study were contributed by four institutions (of the five contributing to TCIA): Memorial Sloan Kettering Cancer Center, The Mayo Clinic, The University of Pittsburgh Medical Center, and Roswell Park Cancer Institute. The cases

Author Manuscript Author Manuscript Author Manuscript Author Manuscript

contributed by each institution were 9 (date range 1999-2002), 5 (1999-2003), 46 (1999-2004), and 31 (1999-2002), respectively. All MRIs were acquired using a standard double breast coil on a 1.5T GE whole-body MRI system (GE Medical Systems, Milwaukee, Wisconsin, USA). Only T1-weighted dynamic contrast-enhanced MR images were used in our current study. The imaging protocols included one pre- and three to five post-contrast images obtained using a T1-weighted 3D spoiled gradient echo sequence with a gadolinium-based contrast agent (Omniscan; Nycomed-Amersham, Princeton, NJ). Typical in-plane resolution was 0.53-0.86 mm, and typical spacing between slices was 2-3 mm.

Three expert board-certified breast radiologists blinded to outcome data independently reviewed each breast MRI examination. Each radiologist identified and annotated the image location of the primary breast tumor and measured maximal tumor diameter using a linear measurement tool. Tumor location on MRI was determined using radiologist reviewer information (via a posteriori consensus). The average maximal diameter as measured by the 3 readers (heretofore called “radiologist size”) was used for comparison to our computer-derived measurements (Figure 1). Each primary breast tumor was then automatically segmented in 3D from the surrounding parenchyma [28].

Extraction of MRI-based computer-extracted image phenotypes

A total of 38 MRI features, each heretofore referred to as a computer-extracted image phenotype (CEIP), were calculated based on the automatically derived 3D tumor segmentations. Since, computationally speaking, many CEIPs can describe a single physical characteristic (such as shape), we divided the CEIPs into six phenotype categories (Figure 2, Supplemental Table 1): 1) **size**—measuring tumor dimensions (4 CEIP), 2) **shape**—quantifying the three-dimensional geometry (3 CEIP), 3) **morphology**—combining shape and margin characteristics such as margin sharpness (3 CEIP), 4) **enhancement texture**—describing the texture of the contrast uptake in the tumor on the first post-contrast MR images (14 CEIP), 5) **kinetic curve assessment**—describing the shape of the kinetic curve and assessing the physiological process of the uptake and washout of the contrast agent in the tumor during the dynamic imaging series (10 CEIP), and 6) **enhancement-variance kinetics**—characterizing the time course of the spatial variance of the enhancement within the tumor (4 CEIP).

We investigated the relationship between “radiologist size” and pathologic stage and lymph node status. We also similarly calculated Pearson correlation coefficients to assess the relationship between pathologic T-stage with “radiologist size” and computer extracted CEIPs from the size category. Actual clinical stage (including T-stage) was not available in our dataset, so we use radiologist size as a surrogate for clinical T-stage. This substitution is reasonable because clinicians commonly use the largest measurement on any imaging modality to establish the T-stage. If MRI is performed, the MRI measurement, often, though not always, informs the clinical T stage.

We assessed five classification tasks. Four tasks involved prediction of pathologic stage: a) stage I versus stage III, b) stage II versus stage III, c) stage I versus stage II, and d) stage I +II versus stage III tumors. The fifth task predicted nodal status: distinguishing between

Author Manuscript Author Manuscript Author Manuscript Author Manuscript

tumors with negative nodes and those with one or more positive nodes. For each of the classification tasks, we determined which single CEIP obtained the best performance in distinguishing between the two sub-groups (e.g. stage I+II versus stage III tumors). Subsequently, for each of the five classification tasks, we determined which CEIP was the next best performer and from a *different* phenotype category than the best performing CEIP. Correlation coefficients were calculated between the first and the second CEIPs to assess whether the CEIPs revealed complementary or largely dependent information. The top 2 CEIPs for each classification task, determined as detailed above, were combined in linear discriminant models (one "2-CEIP model" for each classification task). We also calculated the Pearson correlation coefficients between the top two CEIPs from different categories (those included in the 2-CEIP models) in order to determine to what extent these variables were related. For the prediction of lymph node status, the CEIPs were also evaluated stratified by radiologist size estimates, our surrogate for clinical T-stage (≤ 2 cm [T1]; >2 to ≤ 5 cm [T2]; or > 5 cm [T3]).

Statistical analysis

Leave-one-out cross-validation was used to train/test the 2-CEIP tumor assessment models for each of the classification tasks. Performance (whether for "radiologist size", single CEIPs, or 2-CEIP models) was evaluated using receiver operating characteristic (ROC) analysis, with the area under the curve (AUC) as the figure of merit, using the semi-parametric 'proper' ROC model [29-31]. We determined statistical significance of differences in AUC through bootstrapping (1000 iterations) using a p-value threshold of 0.05 to indicate statistical significance for a single comparison. We corrected for multiple comparisons using the Holm-Bonferroni method.[32]

Results

Patient Population

Ninety-one breast MRIs in patients with biopsy-proven invasive tumors met our inclusion criteria (Table 1 and Table 2). The included invasive carcinomas demonstrated a preponderance of estrogen and progesterone receptor positivity (85% and 79%, respectively). Though the human epidermal growth factor receptor type 2 (HER-2) status was known in only 69% (63/91) of cases, and the majority of these were HER-2 negative (49/63, 78%) as compared to HER-2 positive (14/63, 22%). Lymph node status was almost equally divided between negative and positive with only one case unknown. No patients were documented to have distant metastatic disease. Tumor stage is outlined in Table 2.

Tumor size analysis

For the 91 tumors, the mean "radiologist size" was 2.41 cm (STD ± 0.91; range 0.78-5.93). There were 36 (39.6%) tumors ≤ 2 cm, 54 (59.3%) > 2 cm but ≤ 5 cm, and 1 tumor (1.1%) > 5 cm. The comparison of radiologist size versus pathologic stage (Figure 3a) and versus lymph node status (Figure 3b) demonstrate that the "radiologist size" alone has limited ability to predict stage or lymph node status (also illustrated by Table 4). The correlation coefficients between the "radiologist size" and the four "computer size" CEIPs ranged from 0.63 (surface area) to 0.79 (effective diameter) all with significant p-values (ranging from

Author Manuscript Author Manuscript Author Manuscript Author Manuscript

10^{-19} to 10^{-11}). Correlation coefficients between pathologic stage and different size estimates: "radiologist size," surface area, maximum linear size, and effective diameter were 0.66, 0.63, 0.61 and 0.61 respectively (p-values 10^{-12}— 10^{-10}).

MRI-based computer-extracted image phenotypes analysis

For all the five classification tasks, the CEIP providing the best distinction was always related to tumor size (Table 3), with the surface area (Figure 4a) being the best performer in three tasks and effective diameter in two tasks. All of the discrimination tasks performed statistically significantly better than chance (AUC=0.50) except for the prediction of lymph node status, for which size-based phenotypes alone (human or computer) failed to demonstrate statistical significance over baseline chance (Table 4). We used box plots to visualize how well the most promising CEIPs were able predict pathologic stage (Figure 4).

The most frequent "next-best performing" CEIP for our selected classification tasks (not in the size category) was enhancement texture homogeneity (Table 3), i.e. the homogeneity of the contrast uptake within the tumor at the first post-contrast time-point, with later stage cancers trending towards a more homogeneous appearance (Figure 4b). For the 2-CEIP models, 3 out of the 5 discrimination tasks showed improvement over size alone preserving AUC statistical significance over chance (Table 4). In addition, the performance of the 2-CEIP for lymph node assessment was moderate (AUC=0.62) and became statistically different from baseline chance (p=0.003)—the AUC using the size alone (either radiologist or computer) was not statistically significantly different than chance (Table 4). Correlation coefficients between the two "top-performing" CEIPs (surface area and effective diameter) and the "next-best-performing" CEIP (homogeneity) revealed that there was a low correlation between surface area and homogeneity r = 0.16 (p = 0.12) but moderate correlation between effective diameter and homogeneity r = 0.31 (p=0.003).

After stratifying by "radiologist size", the CEIP most promising for the distinction between tumors ≤2cm with positive and negative lymph nodes, respectively, was irregularity, a morphological feature (AUC=0.73, Figure 4c). Irregularity, however, had little if any discriminatory capabilities for larger tumors (>2cm and ≤5cm). For those larger tumors, the best performing CEIP was enhancement texture homogeneity (AUC=0.74, Figure 4d). Homogeneity, in turn, added no benefit in identifying node status for small lesions ≤2cm.

Discussion

Our results demonstrate that computer-extracted image phenotypes (CEIP) of invasive breast cancer derived from MRI examinations has the potential to help predict pathologic stage. As expected, tumor size metrics (extracted by either the human or the computer) consistently appeared as the most powerful predictor of pathologic stage. We saw a non-significant trend that computer extracted CEIPs related to size were superior to the human extracted size, perhaps because these features are highly correlated with each other as well as pathologic stage. Importantly, we found another, more biologic phenotype—enhancement texture homogeneity—consistently exhibited discriminative ability for pathologic stage. It is important to note that this enhancement texture phenotype describes the homogeneity of the contrast agent distribution, i.e., pattern, within the tumor at a specific (the first post-contrast)

Author Manuscript Author Manuscript Author Manuscript Author Manuscript

time point. Further stratification by tumor size demonstrated that homogeneity predicted lymph node status well in larger tumors while “irregularity,” another CEIP, was more predictive in smaller tumors.

Tumor size is an important part of clinical stage and thus it is consistent that tumor size measurements as determined by the computer perform well in the prediction of pathologic stage. Clinicians routinely use the single largest tumor measurement (either on imaging or clinical exam) to determine the “T-stage.” It is interesting to note that, the best computer-extracted size measurement was “surface area” or “effective diameter” (the diameter of a sphere with the same volume as the lesion) (Table 3) rather than “maximum linear size”, which most closely resembles the radiologists' linear tumor measurement. This result makes sense because a linear tumor size measurement in one dimension does not fully represent the 3D tumor structure and hence has limitations as an indicator for actual tumor burden. It is also noteworthy that homogeneity of contrast uptake is more predictive of pathologic stage than other biologically-related variables and was not well correlated with size CEIPs (thus adding unique predictive power). Increased enhancement texture homogeneity was associated with increased tumor stage. A physiologic explanation for the homogeneity of stage III cancers is their increased microvascular density, compared to stage I and II cancers. Increased microvascular density is the sequelae of tumor related angiogenesis, which, in the absence of central necrosis, allows for rapid and evenly-distributed contrast uptake in the entire tumor (Figure 5)[33,34]. In smaller tumors, where the microvascular density is less, the homogeneity CEIP, and thus angiogenesis, may be less important while morphologic CEIPs, like irregularity, conveying an invasive growth pattern, may dominate in predictive tasks with regard to pathologic stage.

We have found no previously published studies using MRI phenotypes to predict pathologic stage, however, two manuscripts outline attempts to predict lymph node status, a related task. Bhooshan et al. found that homogeneity as well as other MRI phenotypes predicted lymph node positivity for women with invasive breast cancers [35]. Loiselle et al. found that MRI phenotypes (total persistent enhancement and volume adjusted peak enhancement) predicted lymph node burden (≥ 4 axillary nodes) in women with a positive sentinel lymph node biopsy [10]. Booshan et al also explored the use of computer extracted MRI phenotypes to augment the prediction of invasive breast cancer grade exhibiting equivalent AUCs to those we found (grade I vs. III, AUC = 0.80; grade II vs. III, AUC = 0.62; and grade I vs. II, AUC = 0.78) [35]. We found that improvement in pathologic stage prediction was most notable when stage III cancers were included in the prediction task. Predicting patients with stage III breast cancer is clinically important because these individuals have a worse prognosis; may require whole-body imaging such at PET-CT to evaluate for metastatic disease; may be considered for neoadjuvant chemotherapy; and surgical management is less straightforward [5]. Breast MRI enhancement texture homogeneity (in larger stage III tumors) and irregularity (in smaller stage I and II tumors) may help to distinguish women of higher stage, particularly if conventional imaging and physical examination are limited such as in the case of dense breasts. Future work will include an analysis of a larger cohort segregated by grade and characteristics for identification of the best combination of predictors through a multivariate linear regression model.

Author Manuscript Author Manuscript Author Manuscript Author Manuscript

Limitations of this study should be considered when interpreting results. Our patient population was predetermined by the inclusion criteria of the TCGA initiative. The TCGA initiative collected pathologic samples in women with large enough tumors to provide the requisite 200-300 mg of tissue needed for the study. Only women who were surgical candidates (i.e. did not have metastatic disease), were eligible for this study. Therefore, our results can only be generalized to this group. Though the TCGA is a select patient population, it is an important and clinically relevant population. Because the majority of women in our cohort had core-biopsy-proven breast cancer and subsequently underwent breast MRI prior to definitive surgical (or any other) therapy, these patients represent the population for which prediction of pathologic stage to determine clinical management is most pertinent. Our patient sample was relatively small because only a limited number of breast MRI examinations are available in the TCGA/TCIA database. Our data set contained only 11 stage III cancers. For this reason, we did not perform automated feature selection but instead used a more targeted approach to CEIP-based model development. Furthermore, it appears that a large number of our breast cancer cases are ER+, PR+ and HER2+ (i.e. likely luminal A or B) [4], thus perhaps limiting the generalizability of our results to these types of tumors. In addition, the MRIs that we analyzed were acquired over a decade ago, raising the possibility that our results may not reflect existing MRI technology, which has advanced substantially in the interval. Given improved spatial resolution, higher signal-to-noise, and more standardized protocols, our results may, therefore, be conservative. We did not have access to clinical stage or patient outcome, therefore, it will be important to verify whether MRI CEIPs augment prediction of clinical course in addition to pathologic stage to truly target personalized care and thus impact important outcomes like morbidity and mortality. Despite these limitations, the TCGA dataset provided a unique opportunity to examine CEIPs from breast MRI examinations from multiple institutions (on the cutting edge of breast MRI technique at the time of data collection) in a clinically relevant patient population.

Conclusions

We found that while tumor size remains important, computer-extracted image phenotype, like enhancement texture homogeneity and irregularity, appear to augment prediction of pathologic stage. To date, breast cancer clinical stage comprises the criteria on which appropriate therapy has been based despite assertions that biologic features should be included in algorithms that drive management [2,3]. While our results do not indicate that MRI features are ready to replace pathologic stage, CEIPs, like texture heterogeneity and irregularity, may have the potential to provide prognostic information to augment pathologic stage or when pathologic stage is not available, for example when women undergo neoadjuvant chemotherapy. Predicting disease behavior and personalizing care based on anatomic as well as biologic imaging features will likely improve outcomes and effectively leverage resources in the pursuit of optimal breast cancer care. In the future, continued investigation of human and computer assessed phenotypes that uniquely characterize tumors will likely play a role in advancing personalized breast cancer care.

Author Manuscript Author Manuscript Author Manuscript Author Manuscript

Supplementary Material

Refer to Web version on PubMed Central for supplementary material.

Acknowledgments

The authors acknowledge the University of Chicago Dean Bridge Fund and support of the National Institutes of Health (grants: R01CA165229, R01LM010921, and K24CA194251).

MLG is a stockholder in R2 technology/Hologic and receives royalties from Hologic, GE Medical Systems, MEDIAN Technologies, Riverain Medical, Mitsubishi and Toshiba. She is a cofounder of and stockholder in Quantitative Insights. KD received royalties from Hologic.

Funding: The authors acknowledge the University of Chicago Dean Bridge Fund and support of the National Institutes of Health (grants: R01CA165229, R01LM010921, K24CA194251, T32 EB002103).

References

1. Lee SC, Jain PA, Jethwa SC, Tripathy D, Yamashita MW. Radiologist's role in breast cancer staging: providing key information for clinicians. Radiographics : a review publication of the Radiological Society of North America, Inc. Mar-Apr;2014 34(2):330–342.
2. Bagaria SP, Ray PS, Sim MS, et al. Personalizing breast cancer staging by the inclusion of ER, PR, and HER2. JAMA surgery. Feb; 2014 149(2):125–129. [PubMed: 24306257]
3. Yi M, Mittendorf EA, Cormier JN, et al. Novel staging system for predicting disease-specific survival in patients with breast cancer treated with surgery as the first intervention: time to modify the current American Joint Committee on Cancer staging system. Journal of clinical oncology : official journal of the American Society of Clinical Oncology. Dec 10; 2011 29(35):4654–4661. [PubMed: 22084362]
4. Trop I, LeBlanc SM, David J, et al. Molecular classification of infiltrating breast cancer: toward personalized therapy. Radiographics : a review publication of the Radiological Society of North America, Inc. Sep-Oct;2014 34(5):1178–1195.
5. [Accessed September 13, 2014] Breast Cancer Version 3.2014. 2014. http://www.nccn.org/professionals/physician_gls/pdf/breast.pdf
6. Boetes C, Mus RD, Holland R, et al. Breast tumors: comparative accuracy of MR imaging relative to mammography and US for demonstrating extent. Radiology. Dec; 1995 197(3):743–747. [PubMed: 7480749]
7. Kvistad KA, Rydland J, Smethurst HB, Lundgren S, Fjosne HE, Haraldseth O. Axillary lymph node metastases in breast cancer: preoperative detection with dynamic contrast-enhanced MRI. European radiology. 2000; 10(9):1464–1471. [PubMed: 10997438]
8. Javid S, Segara D, Lotfi P, Raza S, Golshan M. Can breast MRI predict axillary lymph node metastasis in women undergoing neoadjuvant chemotherapy. Annals of surgical oncology. Jul; 2010 17(7):1841–1846. [PubMed: 20143266]
9. Mortellaro VE, Marshall J, Singer L, et al. Magnetic resonance imaging for axillary staging in patients with breast cancer. Journal of magnetic resonance imaging : JMRI. Aug; 2009 30(2):309–312. [PubMed: 19466713]
10. Loiselle C, Eby PR, Kim JN, et al. Preoperative MRI improves prediction of extensive occult axillary lymph node metastases in breast cancer patients with a positive sentinel lymph node biopsy. Academic radiology. Jan; 2014 21(1):92–98. [PubMed: 24331270]
11. Berg WA, Gutierrez L, NessAiver MS, et al. Diagnostic accuracy of mammography, clinical examination, US, and MR imaging in preoperative assessment of breast cancer. Radiology. Dec; 2004 233(3):830–849. [PubMed: 15486214]
12. Chen W, Giger ML, Bick U, Newstead GM. Automatic identification and classification of characteristic kinetic curves of breast lesions on DCE-MRI. Med Phys. Aug; 2006 33(8):2878–2887. [PubMed: 16964864]

Author Manuscript Author Manuscript Author Manuscript Author Manuscript

13. Chen W, Giger ML, Lan L, Bick U. Computerized interpretation of breast MRI: investigation of enhancement-variance dynamics. Med Phys. May; 2004 31(5):1076–1082. [PubMed: 15191295]
14. Chen W, Giger ML, Li H, Bick U, Newstead GM. Volumetric texture analysis of breast lesions on contrast-enhanced magnetic resonance images. Magnetic resonance in medicine : official journal of the Society of Magnetic Resonance in Medicine/Society of Magnetic Resonance in Medicine. Sep; 2007 58(3):562–571.
15. Chen W, Giger ML, Newstead GM, et al. Computerized assessment of breast lesion malignancy using DCE-MRI robustness study on two independent clinical datasets from two manufacturers. Acad Radiol. Jul; 2010 17(7):822–829. [PubMed: 20540907]
16. Agner SC, Rosen MA, Englander S, et al. Computerized Image Analysis for Identifying Triple-Negative Breast Cancers and Differentiating Them from Other Molecular Subtypes of Breast Cancer on Dynamic Contrast-enhanced MR Images: A Feasibility Study. Radiology. Jul; 2014 272(1):91–99. [PubMed: 24620909]
17. Youk JH, Son EJ, Chung J, Kim JA, Kim EK. Triple-negative invasive breast cancer on dynamic contrast-enhanced and diffusion-weighted MR imaging: comparison with other breast cancer subtypes. European radiology. Aug; 2012 22(8):1724–1734. [PubMed: 22527371]
18. Golden DI, Lipson JA, Telli ML, Ford JM, Rubin DL. Dynamic contrast-enhanced MRI-based biomarkers of therapeutic response in triple-negative breast cancer. Journal of the American Medical Informatics Association : JAMIA. Nov-Dec;2013 20(6):1059–1066. [PubMed: 23785100]
19. Lehmann BD, Pietenpol JA. Identification and use of biomarkers in treatment strategies for triple-negative breast cancer subtypes. The Journal of pathology. Jan; 2014 232(2):142–150. [PubMed: 24114677]
20. Mazurowski MA, Zhang J, Grimm LJ, Yoon SC, Silber JI. Radiogenomic Analysis of Breast Cancer: Luminal B Molecular Subtype Is Associated with Enhancement Dynamics at MR Imaging. Radiology. Jul 15.2014 :132641.
21. Blaschke E, Abe H. MRI phenotype of breast cancer: Kinetic assessment for molecular subtypes. Journal of magnetic resonance imaging : JMRI. Oct; 2015 42(4):920–924. [PubMed: 25758675]
22. Makkat S, Luypaert R, Stadnik T, et al. Deconvolution-based dynamic contrast-enhanced MR imaging of breast tumors: correlation of tumor blood flow with human epidermal growth factor receptor 2 status and clinicopathologic findings--preliminary results. Radiology. Nov; 2008 249(2):471–482. [PubMed: 18780825]
23. Ashraf AB, Daye D, Gavenonis S, et al. Identification of Intrinsic Imaging Phenotypes for Breast Cancer Tumors: Preliminary Associations with Gene Expression Profiles. Radiology. Apr 4.2014 : 131375.
24. Yamamoto S, Han W, Kim Y, et al. Breast Cancer: Radiogenomic Biomarker Reveals Associations among Dynamic Contrast-enhanced MR Imaging, Long Noncoding RNA, and Metastasis. Radiology. May; 2015 275(2):384–392. [PubMed: 25734557]
25. Mussurakis S, Buckley DL, Horsman A. Prediction of axillary lymph node status in invasive breast cancer with dynamic contrast-enhanced MR imaging. Radiology. May; 1997 203(2):317–321. [PubMed: 9114081]
26. Bhooshan N, Giger ML, Jansen SA, Li H, Lan L, Newstead GM. Cancerous breast lesions on dynamic contrast-enhanced MR images: computerized characterization for image-based prognostic markers. Radiology. Mar; 2010 254(3):680–690. [PubMed: 20123903]
27. Zhu Y, Qiu P, Ji Y. TCGA-assembler: open-source software for retrieving and processing TCGA data. Nature methods. Jun; 2014 11(6):599–600. [PubMed: 24874569]
28. Chen W, Giger ML, Bick U. A fuzzy c-means (FCM)-based approach for computerized segmentation of breast lesions in dynamic contrast-enhanced MR images. Acad Radiol. Jan; 2006 13(1):63–72. [PubMed: 16399033]
29. Metz CE, Pan X. “Proper” Binormal ROC Curves: theory and Maximum-Likelihood Estimation. J Math Psychol. Mar; 1999 43(1):1–33. [PubMed: 10069933]
30. Pan X, Metz CE. The “proper” binormal model: parametric receiver operating characteristic curve estimation with degenerate data. Acad Radiol. May; 1997 4(5):380–389. [PubMed: 9156236]
31. Pesce LL, Metz CE. Reliable and computationally efficient maximum-likelihood estimation of “proper” binormal ROC curves. Acad Radiol. Jul; 2007 14(7):814–829. [PubMed: 17574132]

Author Manuscript Author Manuscript Author Manuscript Author Manuscript

32. Holm S. A simple sequentially rejective multiple test procedure. Scandinavian journal of statistics. 1979:65–70.

33. Buadu LD, Murakami J, Murayama S, et al. Breast lesions: correlation of contrast medium enhancement patterns on MR images with histopathologic findings and tumor angiogenesis. Radiology. Sep; 1996 200(3):639–649. [PubMed: 8756909]

34. Tuncbilek N, Unlu E, Karakas HM, Cakir B, Ozyilmaz F. Evaluation of tumor angiogenesis with contrast-enhanced dynamic magnetic resonance mammography. The breast journal. Sep-Oct;2003 9(5):403–408. [PubMed: 12968962]

35. Bhooshan N, Giger M, Edwards D, et al. Computerized three-class classification of MRI-based prognostic markers for breast cancer. Physics in medicine and biology. Sep 21; 2011 56(18):5995–6008. [PubMed: 21860079]

Author Manuscript Author Manuscript Author Manuscript Author Manuscript

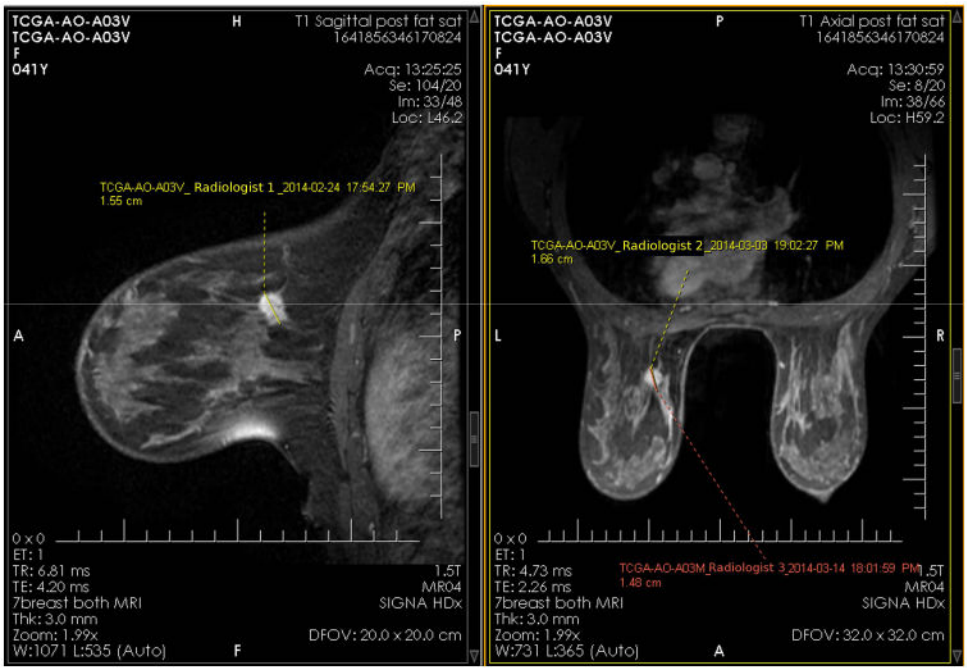

Figure 1.

Representative breast MRI case depicting a sagittal fat saturated T1-weighted image with an annotation identifying the tumor and measurement (“radiologist-size”).

Author Manuscript Author Manuscript Author Manuscript Author Manuscript

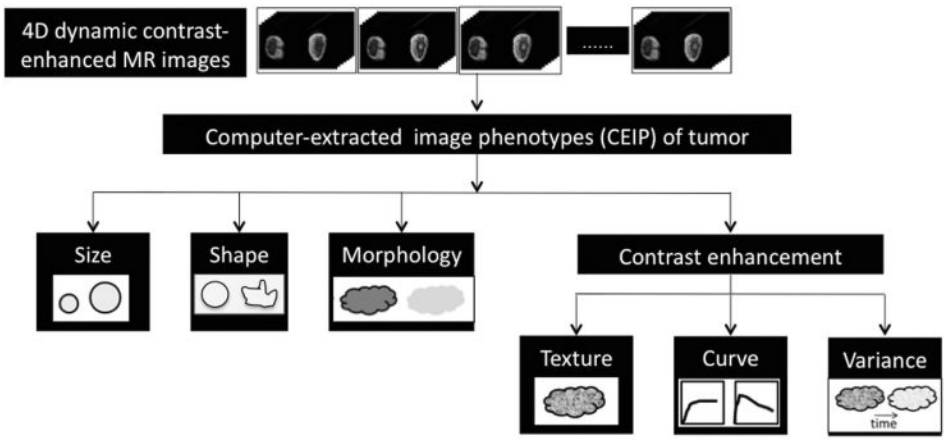

Figure 2. Schematic of the MRI-based computer-extracted image phenotypes

Author Manuscript Author Manuscript Author Manuscript Author Manuscript

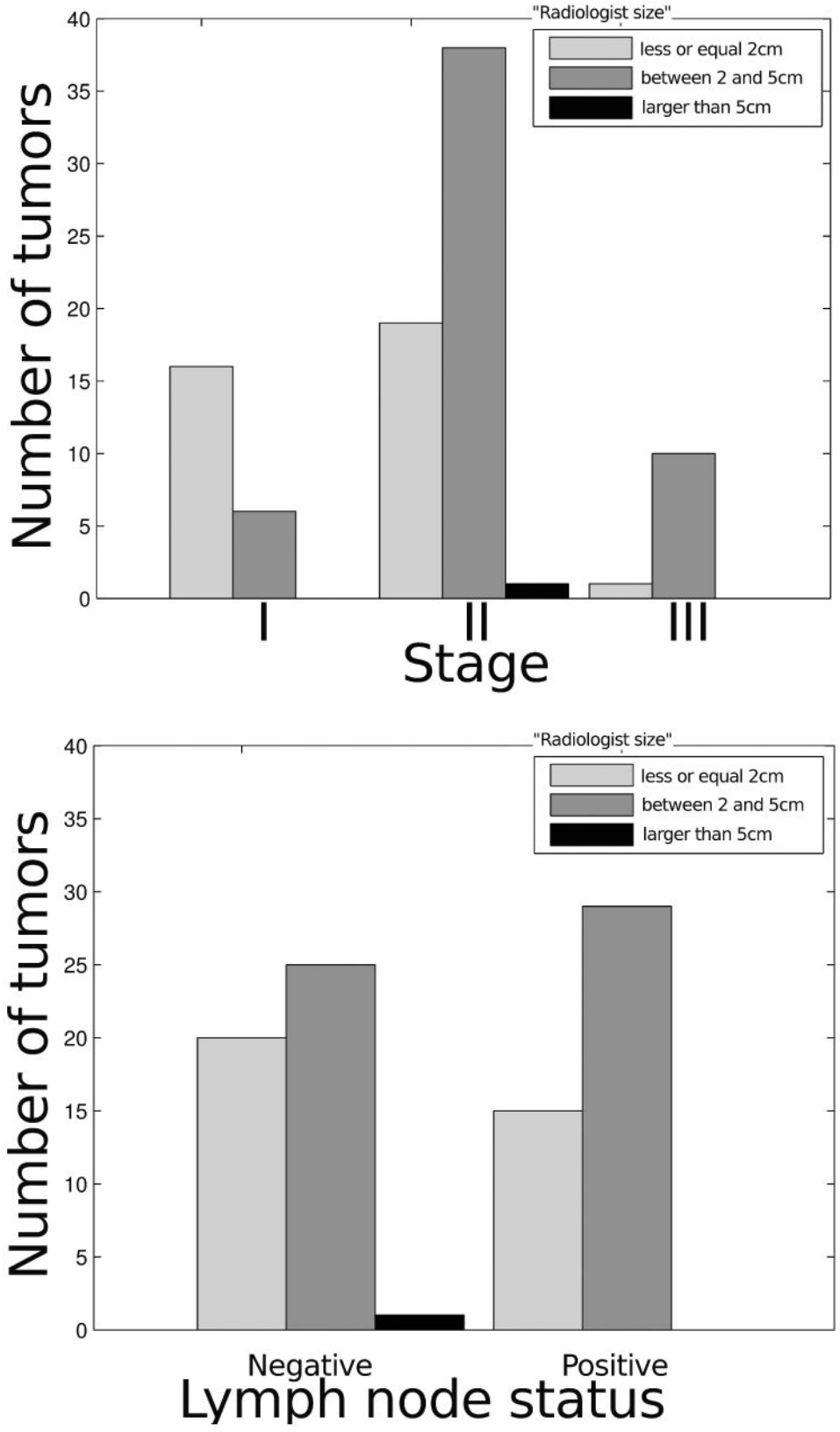

Figure 3.

Author Manuscript Author Manuscript Author Manuscript Author Manuscript

The “radiologist size” distribution (the mean value for the maximal tumor diameter assigned by the 3 expert radiologists) for a) pathologic stage, and b) pathologic lymph node status.

Author Manuscript Author Manuscript Author Manuscript Author Manuscript

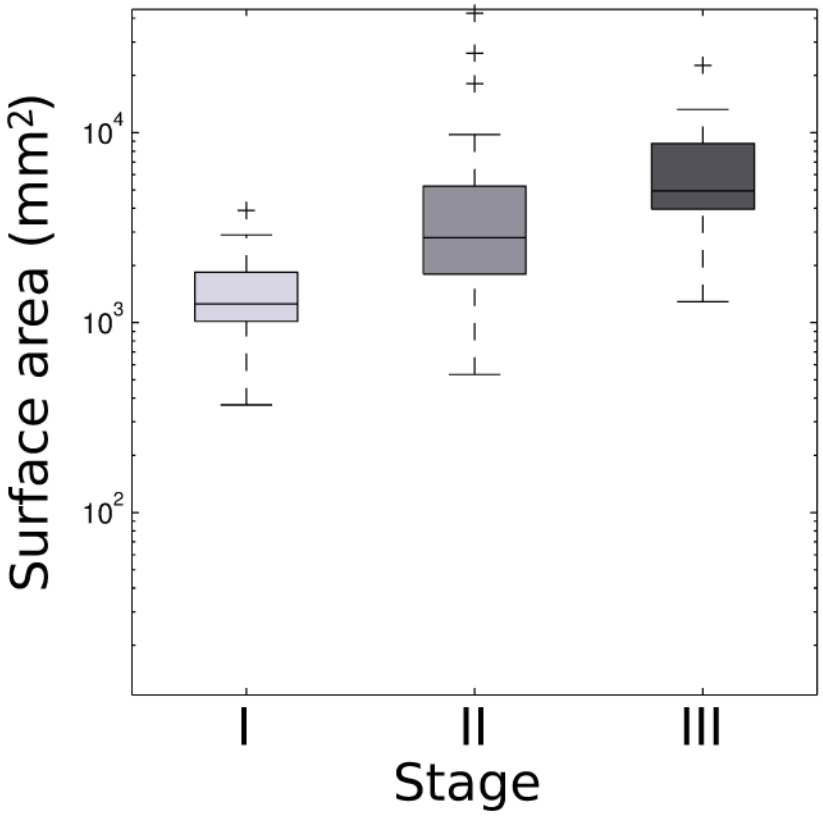

Author Manuscript Author Manuscript Author Manuscript Author Manuscript

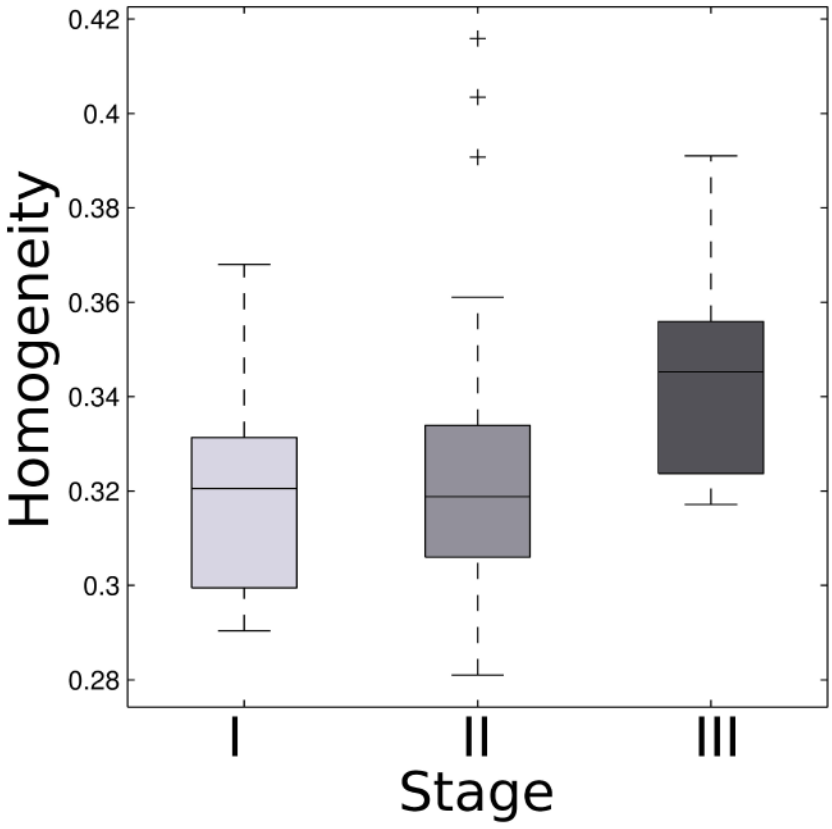

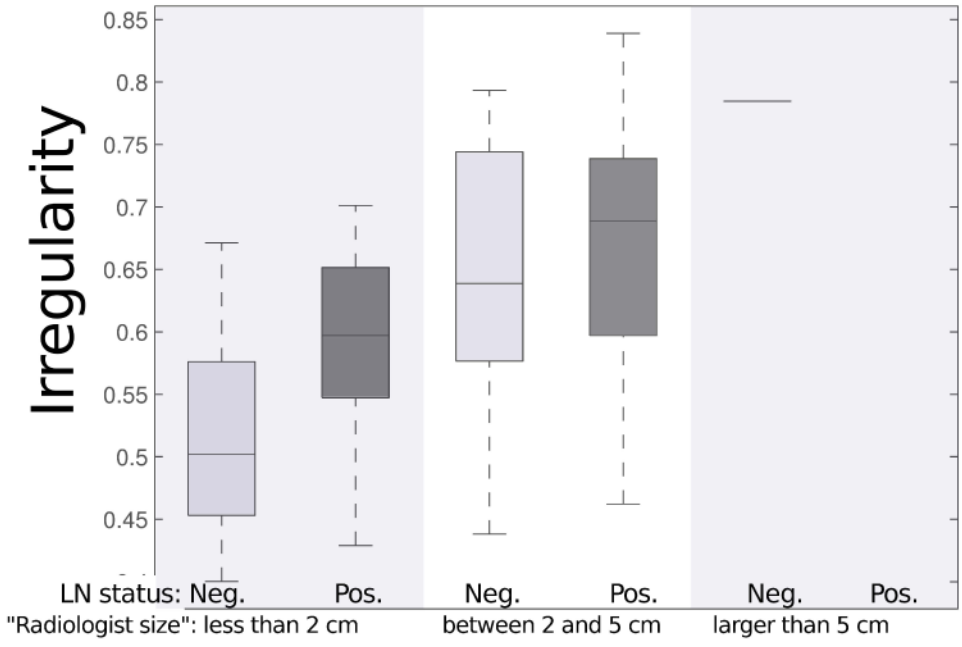

Author Manuscript Author Manuscript Author Manuscript Author Manuscript

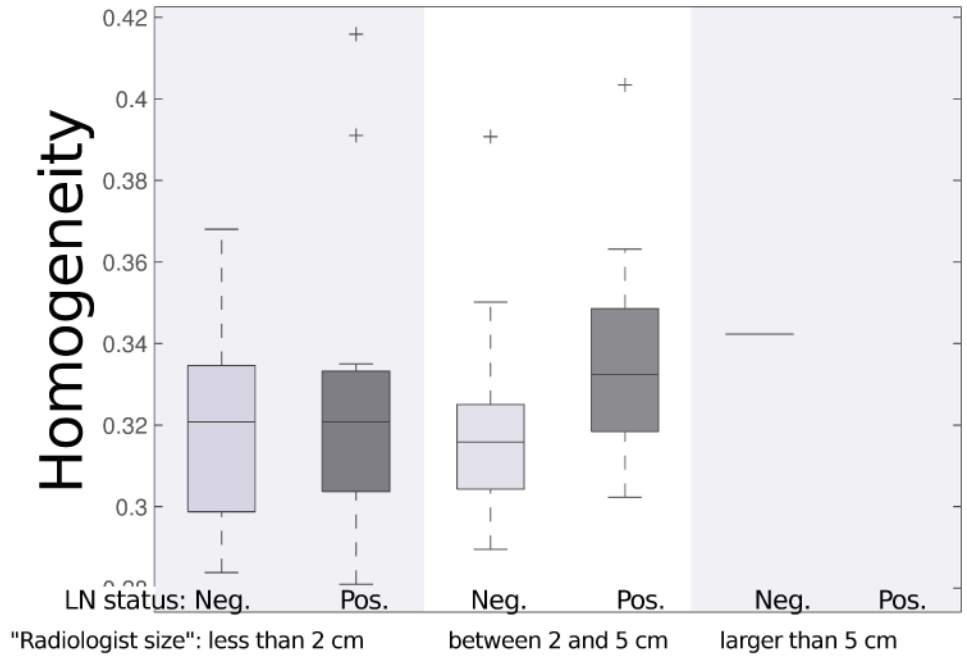

Figure 4.

Distribution of CEIP values for pathologic stage: a) surface area, b) enhancement texture homogeneity (the inverse difference moment of the gray-level co-occurrence matrix calculated within the tumor at the first post-contrast image), and distribution of CEIP for “radiologist size” stratified by pathologic lymph node (LN) status c) irregularity, and d) enhancement texture homogeneity

Author Manuscript Author Manuscript Author Manuscript Author Manuscript

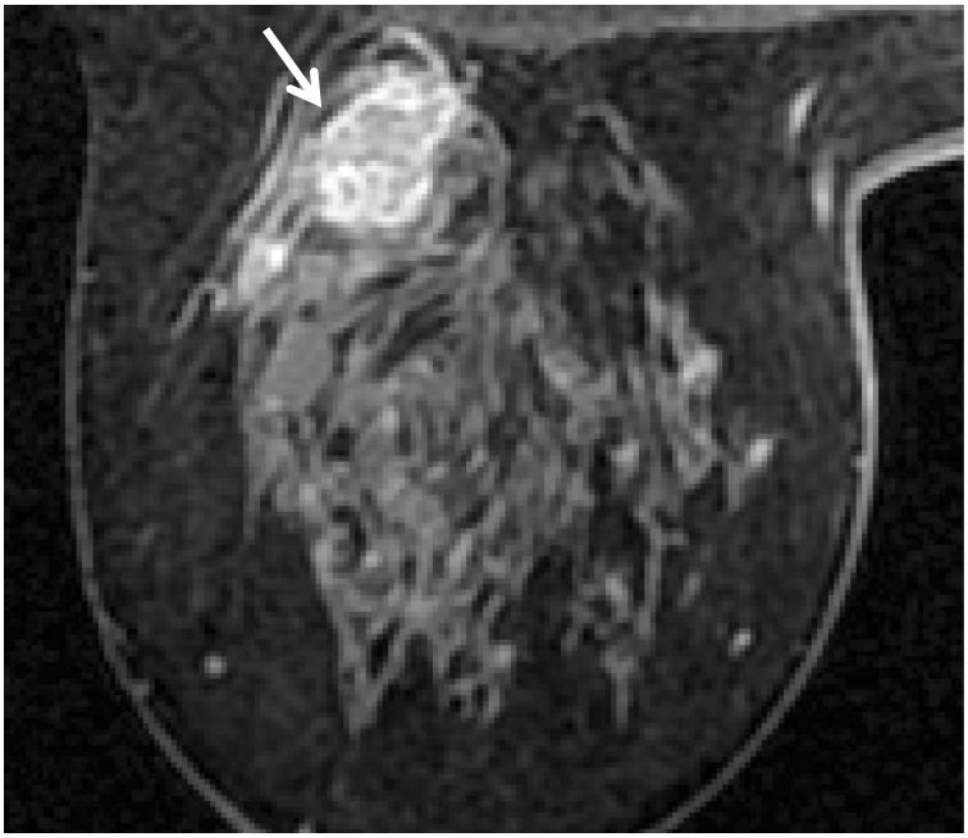

Author Manuscript Author Manuscript Author Manuscript Author Manuscript

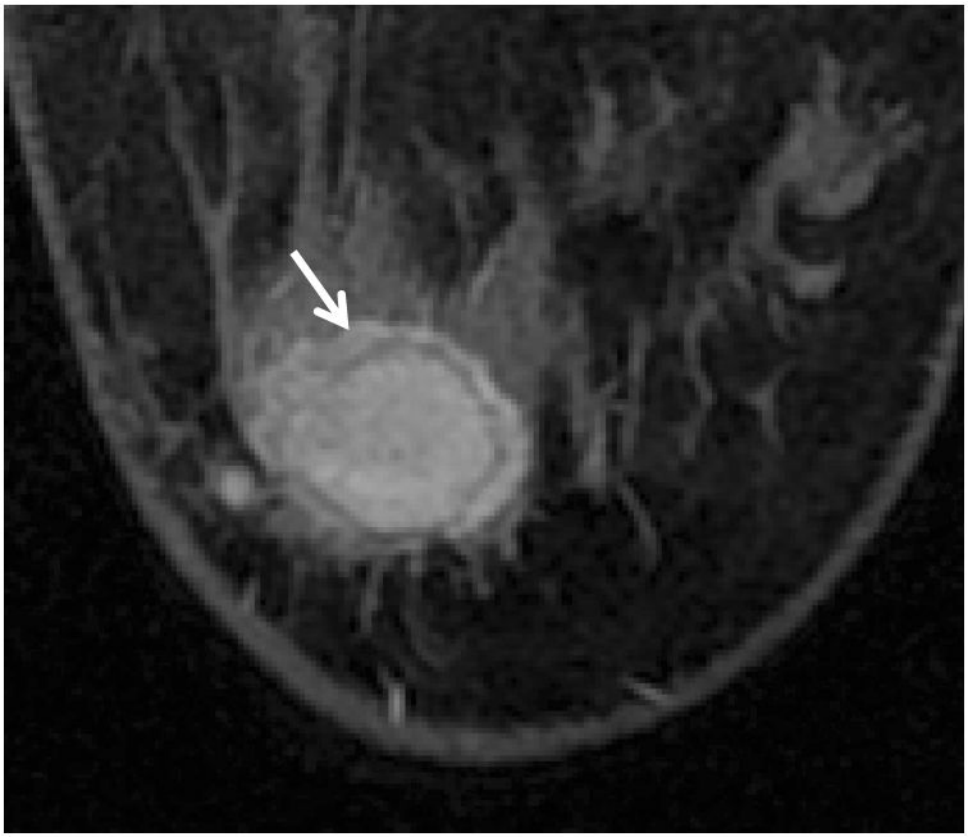

Figure 5.

Example dynamic contrast-enhanced images of primary tumor (both pathologic stage II) at the first post-contrast time point: a) demonstrates a tumor proven to be lymph node negative with “low” enhancement texture homogeneity (imaged at 1 minute, 29 seconds post-contrast), and b) demonstrates a tumor proven to be lymph node positive with “high” enhancement texture homogeneity (imaged at 1 minute, 16 seconds post-contrast).

Author Manuscript

Author Manuscript

Author Manuscript

Author Manuscript

Table 1

Population demographics.

Patient characteristics		
Gender		Female
Age		53.6 (±11.5) years (range 29—82 years)
Tumor characteristics		
Origin	Ductal	86.8% (79/91)
	Lobular	11.0% (10/91)
	Other/mixed	2.2% (2/91)
Estrogen receptor (ER)	positive	84.6% (77/91)
	negative	15.4% (14/91)
Progesterone receptor (PR)	positive	79.1% (72/91)
	negative	2.9% (19/91)
Human epidermal growth factor receptor 2 (HER2)	positive	15.4% (14/91)
	negative	53.8% (49/91)
	undetermined	30.8% (28/91)
Lymph node status	positive	48.4% (44/91)
	negative	50.5% (46/91)
	unknown	1.1% (1/91)

Author Manuscript Author Manuscript Author Manuscript Author Manuscript

Table 2

Pathologic T,N, and stage (note that percentages may not add up to exactly 100% due to rounding)

Pathologic T	
T1	4.4% (4/91)
T1b	3.3% (3/91)
T1c	34.1% (31/91)
T2	54.9% (50/91)
T3	3.3% (3/91)
Pathologic N	
N0	36.3% (33/91)
N0 (i-)	12.1% (11/91)
N0 (i+)	2.2% (2/91)
N1	7.7% (7/91)
N1a	24.2% (22/91)
N1mi	5.5% (5/91)
N2	1.1% (1/91)
N2a	5.5% (5/91)
N3	2.2% (2/91)
N3a	2.2% (2/91)
NX	1.1% (1/91)
Pathologic stage	
I	19.8% (18/91)
IA	4.4% (4/91)
II	1.1% (1/91)
IIA	44.0 (40/91)
IIB	18.7 (17/91)
IIIA	7.7% (7/91)
IIIB	0% (0/91)
IIIC	4.4% (4/91)

Author Manuscript

Author Manuscript

Author Manuscript

Author Manuscript

Table 3

Stage and lymph node classification tasks: Computer-extracted image phenotypes with the best performance in predicting pathological stage and lymph node (LN) status.

Task	Computer-extracted image phenotypes	
	Best performing	**Next-best performing and of different phenotype category**
Stage I vs. III (N=33)	Size: surface area	Morphological: resemblance to radial pattern
Stage II vs. III (N=69)	Size: effective diameter	Enhancement texture: homogeneity
Stage I vs. II (N=80)	Size: surface area	Shape: irregularity
Stage I+II vs. III (N=91)	Size: effective diameter	Enhancement texture: homogeneity
LN status (N=90)	Size: surface area	Enhancement texture: homogeneity

Author Manuscript

Author Manuscript

Author Manuscript

Author Manuscript

Table 4

Stage and lymph node classification tasks: The performance of a) “radiologist size”, which is the average of measurements performed by three breast radiologists, b) “computer size”, which is the best-performing MRI-based computer-extracted image phenotype (CEIP) of the size category, and c) “computer size + biology”, which is the 2-CEIP model based on the best performing CEIPs (Table 3), with all AUC values significantly better than baseline chance (AUC=0.50, with $p \leq 0.003$, i.e., 15 comparisons at 0.05 confidence level) except where noted

Task	AUC (±standard error)		
	“Radiologist size”	**“Computer size”**	**“Computer size + biology”**
Stage I vs. III (N=33)	0.79 (±0.07)	0.88 (±0.06)	0.88 (±0.06)
Stage II vs. III (N=69)	0.60 (±0.08)	0.67 (±0.08)	0.80 (±0.07)
Stage I vs. II (N=80)	0.69 (±0.06)	0.73 (±0.07)	0.73 (±0.07)
Stage I+II vs. III (N=91)	0.65 (±0.08)	0.74 (±0.07)	0.83 (±0.06)
LN status (N=90)	0.53 (±0.05)†	0.55 (±0.06)†	0.62 (±0.05)

† $p \gg 0.05$ with respect to AUC=0.50